TECHNICAL TRANSACTIONS | **CZASOPISMO TECHNICZNE**
CHEMISTRY | CHEMIA
2-Ch/2014

MAREK DOMAŃSKI*, JOANNA KARCZ*

NUMERICAL STUDY OF HYDRODYNAMICS IN AN AGITATED VESSEL EQUIPPED WITH ECENTRICALLY LOCATED HIGH-SPEED IMPELLER

BADANIA NUMERYCZNE HYDRODYNAMIKI W MIESZALNIKU Z NIECENTRYCZNYM MIESZADŁEM SZYBKOOBROTOWYM

Abstract

In this study the results of numerical simulations of hydrodynamics in an agitated vessel with eccentrically located impeller (HE3 or propeller) are presented. Mathematical model of the velocity field is based on Navier-Stocks equation. Characteristics of turbulent flow of liquid is described with the use of CFD methods. In this work the Scale Adaptive Simulation approach coupled with Sliding Mesh method is used. The time-dependent simulations were carried out with ANSYS 14 CFX software.

Keywords: *agitated vessel*, *eccentric impeller*, *CFD*, *SAS-SST*

Streszczenie

W artykule przedstawiono wyniki symulacji numerycznych hydrodynamiki w mieszalniku z niecentrycznie zbudowanym mieszadłem (HE3 lub śmigłowym). Model matematyczny pola prędkości w aparacie oparty został o równania Naviera-Stocksa. Przepływ burzliwy cieczy został opisany za pomocą modelu burzliwości SAS-SST (*Scale Adaptive Simulation – Shear Stress Transport*). Symulacje nieustalone w czasie przeprowadzono przy zastosowaniu oprogramowania ANSYS 14 CFX.

Słowa kluczowe: *mieszalnik*, *mieszadło niecentryczne*, *CFD*, *SAS-SST*

* M.Sc. Eng. Marek Domański, Prof. Joanna Karcz, Department of Chemical Engineering, Faculty of Chemical Engineering, West Pomeranian University of Technology, Szczecin.

1. Introduction

In industry the agitated vessels with eccentrically located impeller are regarded as alternative solution to agitated vessels with centrally located impeller with mounted baffles [1]. Eccentricity e is defined as the distance between the axis of agitated vessel and axis of impeller shaft. Location of impeller shaft in eccentric position causes the breakage of primary vortex observed in apparatus with centrally located impeller and promotion of mixing in microscale [2]. This solution is particularly appreciated in industries, where high level of apparatus cleanness is a key factor, such as food or pharmaceutical industry. The simple construction of agitated vessel with eccentrically mounted impeller helps in cleaning and conservation [3]. In agitated system containing a shear sensitive material, such as growing crystals or biological origin material, baffles could damage this type of material and have negative impact on overall process yield. This effect is not observed in agitated vessel with eccentrically located impeller, which are devoid of baffles [4]. Those types of agitated vessels are also often used in production processes of paints and varnishes. Moving the impeller shaft into eccentric position causes the increase in flow instabilities and axial mixing, what helps to destroy regions of poor mixing, which are characteristic for laminar agitation or agitation of viscous liquid [5].

In the literature, it could be found a lot of experimental studies of hydrodynamics, mixing time or heat transfer process in a wall region for agitated vessels with eccentrically located impeller, but still there is not many studies about numerical simulation of such systems, especially those characterized by Reynolds number higher than $\mathrm{Re} = 10^4$ (turbulent agitation).

The aim of this study is to analyse of numerically modeled hydrodynamics for agitated vessel with eccentrically located down-pumping HE 3 impeller or up-pumping propeller. Shaft eccentricity for tested cases was equal $e/R = 0.4$.

2. Range of numerical simulations

Using CFD methods the hydrodynamics for agitated vessel of inner diameter $T = 2R = 0.3$ m was modeled. The agitated vessel was filled up with liquid to the height $H = T$. The modeled liquid had physical properties of water. In the agitated vessel, on the height $h = 0.33$ from tank bottom HE3 impeller with diameter $D = 0.33T$ was located. The agitated vessel equipped with propeller with diameter $D = 0.33T$ and pitch $S = D$ was also tested. The eccentricity of impeller shaft was equal $e = 0.4R$. Speed of impeller was set to $n = 7.5$ 1/s. Reynolds number calculated for those systems is equal $\mathrm{Re} = 6.3 \cdot 10^4$. Geometry of the system with HE3 impeller is presented in Fig. 1.

The numerical mesh was created for two zones: for cylindrical, moving zone around the impeller and for the rest of bulk volume of the liquid (Fig. 1b, c). Numerical mesh for system with HE3 impeller consists of over 870000 elements while numerical mesh for system with propeller consists of over 740000 elements. The grid convergence index $\mathrm{GCI}_{\mathrm{fine}}$ was calculated according to procedure recommended by Celik [6]. The $\mathrm{GCI}_{\mathrm{fine}}$ index was equal 6,18% for numerical grid of system with propeller and 9.03% for numerical grid of system with HE3 impeller.

Numerical simulations for both variants of the agitated vessel were carried out with ANSYS 14 CFX software. The hydrodynamics was modeled with the use of Reynolds averaged Navier-Stocks equation. The turbulent nature of the flow was described using turbulence model SAS-SST (Scale Adaptive Simulation – Shear Stress Transport). Rotation of impeller swept zone was described with sliding mesh approach.

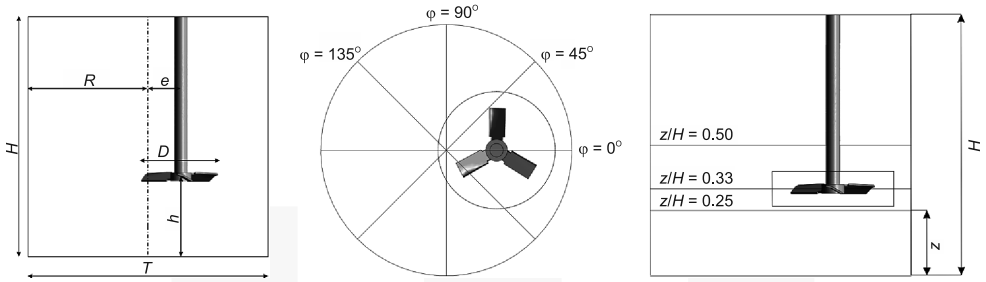

Fig. 1. Geometry of agitated vessel with eccentric HE3 impeller

The SAS-SST turbulence model divides flow into two regions. The steady flow region is modeled with the use of Shear Stress Transport (SST) turbulence model while the unsteady flow region is modeled "LES-like" way with the use of von Karman length-scale. This division is obtained by adding additional source term Q_{SAS} into turbulent frequency transport equation in SST model [7, 8]:

$$\frac{\partial \rho k}{\partial t}+\frac{\partial}{\partial x_j}(\rho w_j k)=P_k-\rho c_{\mu} k\omega+\frac{\partial}{\partial x_j}\left[\left(\mu+\frac{\mu_t}{\sigma_k}\right)\frac{\partial k}{\partial x_j}\right] \tag{1}$$

$$\frac{\partial \rho \omega}{\partial t}+\frac{\partial}{\partial x_j}(\rho w_j \omega)=\alpha\frac{\omega}{k}P_k-\rho\beta\omega^2+Q_{\mathrm{SAS}}+\frac{\partial}{\partial x_j}\left[\left(\mu+\frac{\mu_t}{\sigma_{\omega}}\right)\frac{\partial \omega}{\partial x_j}\right]+ +(1-F_1)\frac{2\rho}{\sigma_{\omega 2}}\frac{1}{\omega}\frac{\partial k}{\partial x_j}\frac{\partial \omega}{\partial x_j} \tag{2}$$

$$Q_{\mathrm{SAS}}=\max\left[\rho\zeta_2\kappa S^2\left(\frac{L}{L_{vK}}\right)^2-C\cdot\frac{2\rho k}{\sigma_{\Phi}}\max\left(\frac{1}{\omega}\frac{\partial \omega}{\partial x_j}\frac{\partial \omega}{\partial x_j},\frac{1}{k^2}\frac{\partial k}{\partial x_j}\frac{\partial k}{\partial x_j}\right),0\right] \tag{3}$$

where:

- ρ – density,
- t – time,
- x – coordinate,
- w – velocity,
- k – turbulence kinetic energy,
- P_k – shear production of turbulence,
- c_{μ}, σ_k – constants,
- ω – turbulence frequency,

μ, μ_t – viscosity and turbulent viscosity,
α, β – constants,
σ_ω, $\sigma_{\omega 2}$ – constants,
F_1 – SST blending function,
ζ_2, σ_Φ, C – constants,
κ – von Karman constant,
S – invariant of the strain rate tensor,
L, L_{vK} – length-scale and von Karman length-scale.

The iterative computations of hydrodynamics model discretized with the use Second Order Euler backward scheme were conducted with HP Z820 workstation. It took $1{,}142 \cdot 10^6$ s in the case of agitated vessel with the propeller and $0{,}934 \cdot 10^6$ s in the case of agitated vessel with the HE3 impeller to simulate 30 s of liquid turbulent flow.

3. Numerical results

The tested agitated vessels are equipped with eccentrically located impeller, due this fact the system characterizes high level of flow asymmetry. Thereby, the numerical results will be presented at three chosen radial planes of dimensionless axial coordinate z/H = (0,25; 0,33; 0,5) (Fig. 1c) and at four chosen axial planes of angular coordinate φ = (0°; 45°; 90°; 135°) (Fig. 1b). Time-averaged liquid flow field for different cross sections of agitated vessel are presented in Fig 2.

Vector of velocity calculated during numerical simulations was decomposed into three velocity components: tangential (Figs. 3, 4), radial (Figs. 5, 6) and axial (Figs. 7, 8) for both

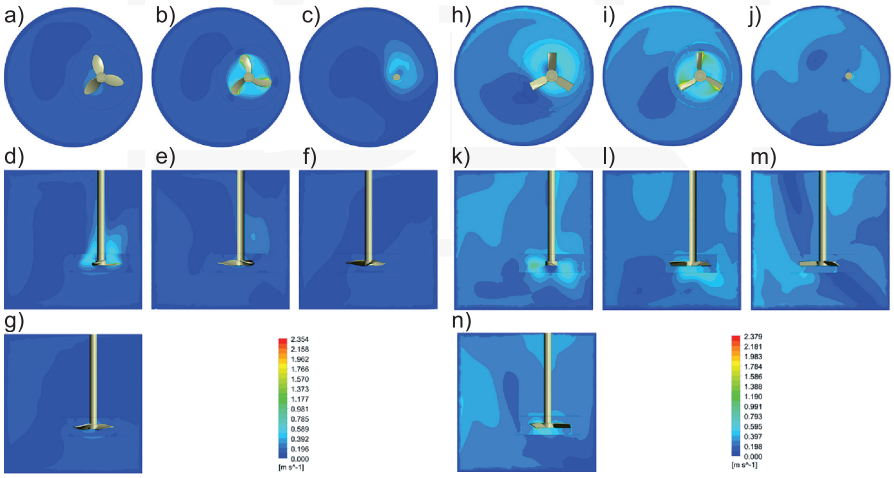

Fig. 2. Contours of time-averaged liquid velocity in the agitated vessel with eccentrically located propeller (a, b, c, d, e, f, g) and HE3 impeller (h, i, j, k, l, m, n) for radial plane and dimensionless axial coordinate a, h) z/H = 0.25, b, i) z/H = 0.33, c, j) z/H = 0.50, as well as for axial plane and angular coordinate d, k) 0°, e, l) 45°, f, m) 90°, g, n) 135°

tested systems. Dimensionless, time-averaged components of velocity vector are presented as radial profiles in the system of dimensionless coordinates. Analysis of those components is conducted for radial planes crossing agitated vessel on three different dimensionless heights: z/H = (0,25; 0,33; 0,50) for four angular coordinates φ = (0°; 45°; 90°; 135°) (Fig. 1b, c).

Positive values of tangential velocity component indicates that liquid is moving in the direction consistent with the direction of impeller rotation. Negative values indicate that this movement is reverse to the direction of the rotation. Axial velocity component allows to conclude whether liquid is flowing into direction of free surface or bottom of the agitated vessel. Positive values of this velocity component indicate that liquid is moving in direction of free surface while negative values indicate reverse direction. When radial component of the velocity is positive liquid is flowing from impeller into direction of the agitated wall. Negative values of this velocity component indicate that the direction of movement is reverse.

Analyzing radial profiles of velocity components for up-pumping propeller and down--pumping HE3 impeller it can be stated that profiles for system equipped with eccentric propeller (Figs. 3, 5, 7) are flatter than profiles for system equipped with eccentric HE3 impeller (Figs. 4, 6, 8).

In the case of the system equipped with the propeller dimensionless tangential velocity (Fig. 3) has low values around 0. The highest values of this velocity component is observed in the vicinity of the propeller in cross-section located on the height of the impeller (z/H = 0,33). The distribution of this velocity component is much more diversified for the agitated vessel with HE3 impeller (Fig. 4). Profiles for this system show that, in the cross--section above impeller (z/H = 0,5) in the region near agitated vessel center (r/R = 0), liquid tends to flow in the direction revers to the direction of impeller rotation. Values of tangential velocity are higher in case of agitated vessel equipped with HE3 impeller than in the case of the same agitated vessel equipped with propeller.

Profiles of the radial velocity for the system equipped with the propeller (Fig. 5) show that in the region opposite to the impeller ($r/R < 0$) radial flow of a liquid almost does not occur. For agitated vessel region where $r/R > 0$, at plane under the impeller (z/H = 0,25) liquid flows in the direction of impeller. In this region, at plane on the height of the impeller (z/H = 0,33) and above it (z/H = 0,5) liquid flows in the direction of the vessel wall. It is consistent with the direction of the propeller pumping. For the agitated vessel with HE 3 impeller (Fig. 6) and profiles under impeller (z/H = 0,25) liquid mostly flows in the direction of the vessel wall. For two other analyzed heights (z/H = 0,33 or 0,5) the impeller sucks liquid in its direction. Analyzing values of radial velocity it can be stated that eccentric HE3 impeller has higher sucking and pumping capacity than propeller of the same size.

Axial flow in the case of axial cross-sections of angular coordinate φ = 90° and 135° in the agitated vessel equipped with the propeller (Fig. 7) almost does not occur. Axial flow is observed in the region of the impeller ($r/R > 0$) mostly for profiles on the height of impeller and above it (z/H = 0,33 or z/H = 0,5). Analyzing profiles of axial velocity for the agitated vessel equipped with HE3 impeller (Fig. 8) it can be stated that in the case of this system this velocity component dominates in liquid flow. The highest values of axial velocity are observed in the vicinity of the impeller at planes located on height z/H = 0,33 and z/H = 0,5.

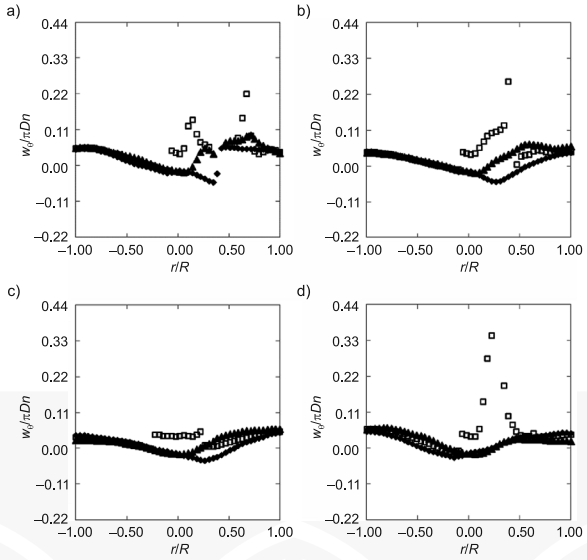

Fig. 3. Radial profiles of dimensionless time-averaged dimensionless tangential velocity component $w_\theta/\pi Dn$ at the plane (a) 0°, (b) 45°, (c) 90°, (d) 135°, for three values of dimensionless axial coordinate z/H (= 0.25 (♦), 0.33 (□), 0.50 (▲)) for system with propeller

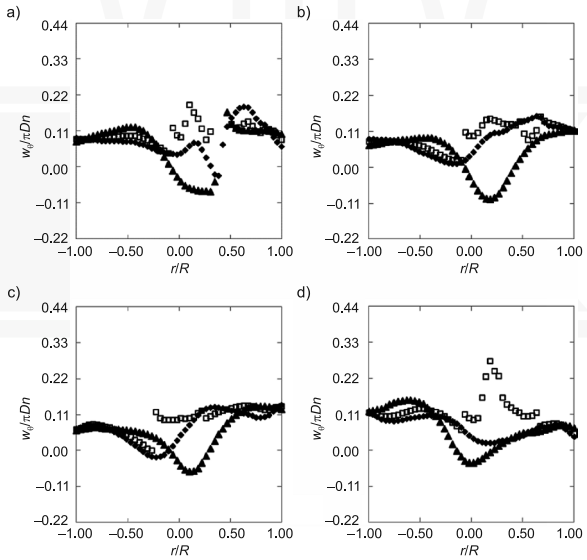

Fig. 4. Radial profiles of dimensionless time-averaged dimensionless tangential velocity component $w_\theta/\pi Dn$ at the plane (a) 0°, (b) 45°, (c) 90°, (d) 135°, for three values of dimensionless axial coordinate z/H (= 0.25 (♦), 0.33 (□), 0.50 (▲)) for system with HE3 impeller

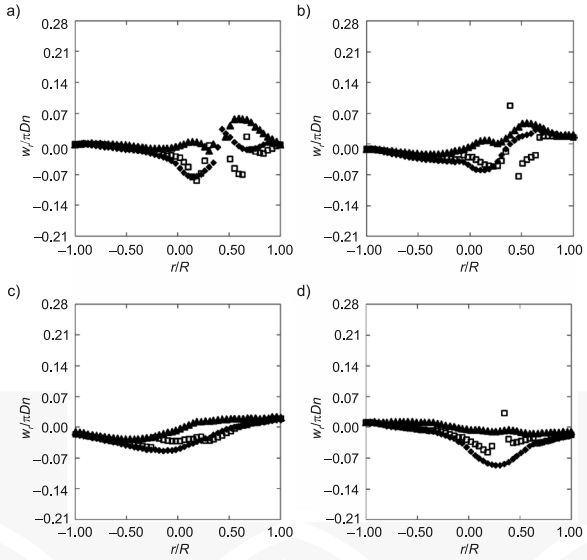

Fig. 5. Radial profiles of dimensionless time-averaged dimensionless radial velocity component $w_r/\pi Dn$ at the plane (a) 0°, (b) 45°, (c) 90°, (d) 135°, for three values of dimensionless axial coordinate z/H (= 0.25 (♦), 0.33 (□), 0.50 (▲)) for system with propeller

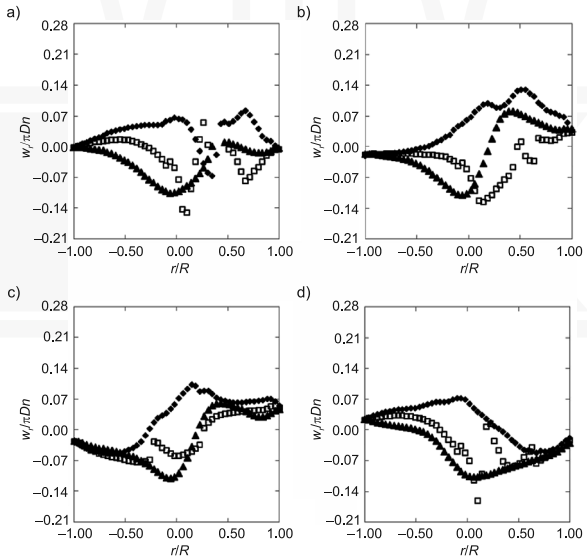

Fig. 6. Radial profiles of dimensionless time-averaged dimensionless radial velocity component $w_r/\pi Dn$ at the plane (a) 0°, (b) 45°, (c) 90°, (d) 135°, for three values of dimensionless axial coordinate z/H (= 0.25 (♦), 0.33 (□), 0.50 (▲)) for system with HE3 impeller

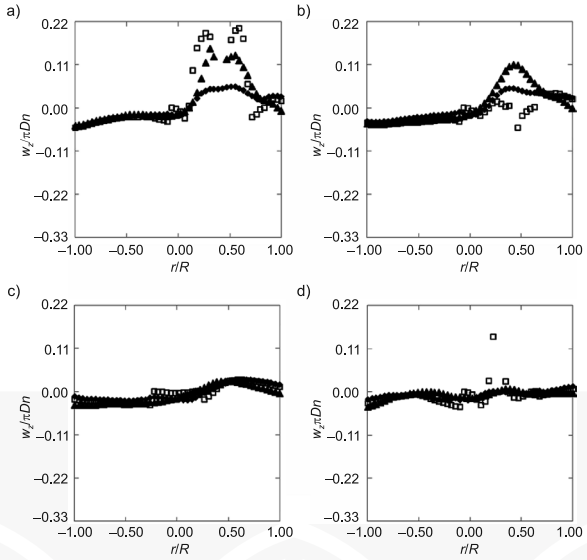

Fig. 7. Radial profiles of dimensionless time-averaged dimensionless axial velocity component $w_z/\pi Dn$ at the plane (a) 0°, (b) 45°, (c) 90°, (d) 135°, for three values of dimensionless axial coordinate z/H (= 0.25 (♦), 0.33 (□), 0.50 (▲)) for system with propeller

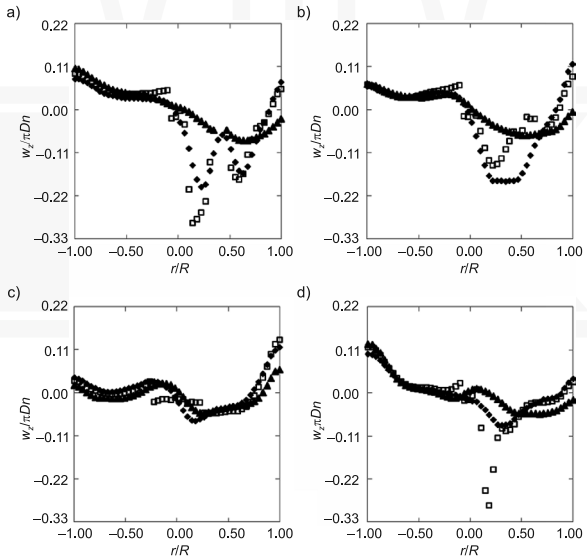

Fig. 8. Radial profiles of dimensionless time-averaged dimensionless axial velocity component $w_z/\pi Dn$ at the plane (a) 0°, (b) 45°, (c) 90°, (d) 135°, for three values of dimensionless axial coordinate z/H (= 0.25 (♦), 0.33 (□), 0.50 (▲)) for system with HE3 impeller

During the numerical simulation of hydrodynamics in the agitated vessel with eccentrically located high-speed impeller the values of power number *Ne* were monitored. In the literature, there can be found two ways of calculation of power number from results of numerical simulations. In the first method [9] power number is calculated with the use of torque value from equation:

$$Ne_M = \frac{2\pi n M}{\rho n^3 D^5} \tag{4}$$

where:

- Ne – power number,
- n – impeller speed,
- M – torque,
- D – impeller diameter.

The second method allows to calculate power number *Ne* form integrated value of turbulence eddy dissipation [10]. Due the fact that values of turbulence eddy dissipation are under predicted in numerical simulation, the first method was chosen to calculate power number. In the case of the agitated vessel equipped with the propeller time-averaged power number was equal Ne_M = 0,12 and in the case of the agitated vessel equipped with HE3 impeller time-averaged power number was equal Ne_M = 0.40. Experimentally measured power numbers for such systems are respectively equal $Ne_{\exp}$ = 0.35 ± 0.05 and $Ne_{\exp}$ = 0.43 ± 0.06 [11]. The difference between values calculated from numerical simulation and those measured experimentally for systems equipped with propeller and HE3 impeller are equal to 65% and 6% respectively.

4. Conclusions

In this study, hydrodynamics for the agitated vessel equipped with the eccentrically located propeller or HE3 impeller was analysed. The computational fluid dynamics method were used to obtain detailed data on the fluid flow in such type of the agitated vessel. The SAS-SST turbulence model coupled with the sliding mesh method were used to conduct numerical simulations. Acquired data were used to create flow field and radial profiles of velocity components.

Power number *Ne* was also analysed. Values of the power number for both tested cases were monitored and gathered in each of 30 000 time-steps during numerical simulation. Those data were used to calculate mean values of power number *Ne*. The difference between power number *Ne* measured experimentally and calculated from the results of simulation is equal 65% for the agitated vessel equipped with eccentrically located propeller and 6% for the agitated vessel equipped with eccentrically located HE3 impeller. Such difference observed for the propeller could be explained by the difference between real geometry of the propeller and geometry created for purpose of numerical simulation. The real geometry of the propeller has some sharp edges and geometry created during numerical analysis has all smooth edges. The fact that sharp edges could create more turbulent flow

is well known. Higher level of the turbulence generated by the propeller could increase power consumption and consequently power number.

Project was financed by the National Science Centre with founds granted on the basis of decision number DEC-2011/03/N/ST8/02822.

References

[1] Stręk F., *Mieszanie i mieszalniki*, WNT, Warsaw 1981.
[2] Galletti C., Pintus S., Brunazzi E., *Effect of shaft eccentricity and impeller blade thickness on the vortices features in an unbaffled vessel*, Chemical Engineering Research & Design, vol. 85(4A), 2009, 391-400.
[3] Galletti C., Brunazzi E., *On the main flow features and instabilities in an unbaffled vessel agitated with an eccentrically located impeller*, Chemical Engineering Science, vol. 63, 2008, 4494-4505.
[4] Sanchez Cervantes M.I., Lacombe J., Muzzio F.J., Alvarez M.M., *Novel bioreactor design for the culture of suspended mammalian cells. Part I: Mixing characterization*, Chemical Engineering Science, vol. 61, 2006, 8075-8084.
[5] Karcz J., Cudak M., Szoplik J., *Stirring of a liquid in a tank with an eccentrically located impeller*, Chemical Engineering Science, vol. 60, 2005, 2369-2380.
[6] Celik I. B., Ghia U., Roache P.J., Freitas Ch.J., Coan H., Raad P.E., *Procedure for Estimation and Reporting of Uncertainty Due to Discretization in CFD Applications*, Journal of Fluid Engineering, vol.130(7), 2008, 078001.
[7] Menter F.R., Egorov Y., *The Scale-Adaptive Simulation Method for Unsteady Turbulent Flow Predictions. Part 1: Theory and Model Description*, Flow Turbulence and Combustion, vol. 85(1), 2010, 113-138.
[8] Egorov Y., Menter F.R., Lechner R., Cokljat D., *The Scale-Adaptive Simulation Method for Unsteady Turbulent Flow Predictions. Part 2: Application to Complex Flows*, Flow Turbulence and Combustion, vol. 85(1), 201, 139-165.
[9] Singh H., Fletcher D.F., Nijdam J.J., *An assessment of different turbulence models for predicting flow in a baffled tank stirred with a Rushton turbine*, Chemical Engineering Science, vol. 66(23), 2011, 5976-5988.
[10] Xuereb C., Bertrand, J., *3-D hydrodynamics in a tank stirred by a double-propeller system and filled with a liquid having evolving rheological properties*, Chemical Engineering Science, vol. 51(10), 1996, 1725-1734.
[11] Cudak M., *Wymiana ciepła i pędu w mieszalniku z niecnetrycznie zabudowanym mieszadłem*, praca doktorska, Politechnika Szczecińska, Szczecin 2004.